ELSEVIER

Optical Materials 13 (2000) 417–425

OPTICAL Materials

Spectroscopy of Er and Er–Yb-doped phosphate glasses

R. Francini [a,*], F. Giovenale [a], U.M. Grassano [a], P. Laporta [b], S. Taccheo [b]

[a] *I.N.F.M., Dipartimento di Fisica, Università di Roma Tor Vergata, via della Ricerca Scientifica 1, 00133 Roma, Italy*
[b] *I.N.F.M., Dipartimento di Fisica del Politecnico di Milano and CEQSE-CNR, Piazza Leonardo da Vinci 32, 20133 Milano, Italy*

Received 1 August 1998; accepted 21 June 1999

Abstract

Optical absorption and emission properties of Er and Er–Yb-doped phosphate glasses are investigated both at low and room temperature in the near infrared spectral region between 800 and 2000 nm, and the results are thoroughly discussed in connection with the expected transitions originating from the crystal-field split $^4I_{15/2}$ and $^4I_{13/2}$ levels of the Er^{3+} ion. Accurate measurements of the $^4I_{13/2}$ fluorescence lifetimes and the determination of the stimulated emission cross section for the Er transition at 1.5 μm are also reported. Excited state absorption (ESA) from the metastable $^4I_{13/2}$ level towards the higher energy levels is measured in the 450–1200 nm spectral region. The ESA absorption peaks are in good agreement with the positions of the higher states of the $4f^{11}$ Er^{3+} manifold.

PACS: 42.70C; 78.55

Keywords: Rare earths; Glasses; Spectroscopy

1. Introduction

The versatility of glasses and the broader emission and absorption spectra they provide, as compared with crystalline hosts, have led to the use of rare earth-doped glasses in many applications, thus stimulating, in the last decade, an increasing interest in their properties from both a spectroscopic (for a recent review, see [1]) and a technological point of view (for recent reviews, see [2,3]). Infrared lasers, optical fibre amplifiers and energy up-converters are the most successful achievements based on the use of these systems as active materials [4–8]. Among the numerous rare earth-doped glass materials, Er-doped glass has attracted much interest, since its first operation as laser material in 1965 [9], for telemetry and laser ranging applications, mostly due to the Er^{3+} ion transition around 1.5 μm, which is an eye-safe wavelength. More recently, with the development of the strained-layer InGaAs laser diodes emitting at 980 nm wavelength, laser physicists have in particular been actively considering continuous wave laser oscillators based on Er^{3+}-doped glasses and optical fibres. This interest was also stimulated by the successful operation of the Er-doped fibre amplifier pumped at 980 nm wavelength [10], which rapidly turned out to be a key component in all modern optical transmission systems.

The $4f^{11}$ electronic configuration of the Er ions is split by the electrostatic and spin–orbit interactions into several manifolds of states. The lowest in

* Corresponding author. Tel.: +39-06-72594505; fax: +39-06-2023507.
E-mail address: francini@roma2.infn.it (R. Francini).

0925-3467/00/$ - see front matter
PII: S0925-3467(99)00095-6

energy are the quartets $^4I_{15/2}$, $^4I_{13/2}$, $^4I_{11/2}$, $^4I_{9/2}$, and the next higher levels are the quartets $^4F_{9/2}$ and $^4S_{3/2}$. All these levels and the other excited states span the near infrared and visible spectrum, thus making the Er^{3+} ion one of the most easily pumped dopants. However, since Er-doped glasses act as three-level gain systems at 1.5 μm, codoping with Yb is often used to enhance the absorption and pumping efficiency in short-length active materials employed in compact laser devices and high power optical amplifiers. In fact, the Yb^{3+} ion has 13 4f electrons and therefore the energy levels are analogous to those of an ion with a single f electron, with inverted order of the spin-orbit levels. The $^2F_{7/2}$ is thus the ground state and the $^2F_{5/2}$ the next excited state of the ion. Because the spectral region of the $^2F_{7/2} \rightarrow {}^2F_{5/2}$ Yb^{3+} transition overlaps that of the $^4I_{15/2} \rightarrow {}^4I_{11/2}$ transition, it is possible to achieve an effective Yb to Er transfer mechanism of the excitation energy [11,12], and in the last few years many authors have successfully demonstrated pulsed as well as continuous wave operation of Er–Yb-doped glass lasers [11,13–16]. In particular, to obtain an effective energy transfer, the back energy transfer process from Er to Yb needs to be minimised by a fast non-radiative multiphonon decay of the Er ions from the $^4I_{11/2}$ pump level to the $^4I_{13/2}$ level. High phonon energy glasses, such as phosphate glasses, enhance the multiphonon decay probability and they are therefore suitable host candidates [1,11]. In spite of the extensive investigations of Er-doped glasses and of the interesting experimental results obtained with Er–Yb-doped phosphate glass lasers, some of the basic spectroscopic properties of these active materials are still not completely clarified.

In this work we focus on three Er–Yb-doped phosphate glasses, which appear to be among the best active materials for bulk and wave-guide lasers as well as for short fibre lasers, having a very high phonon energy and, consequently, a higher energy transfer efficiency. In order to characterise the spectroscopic properties of Er- and Er–Yb-doped phosphate glasses following parameters were measured in samples with different concentrations of dopant and codopant ions at different temperatures: (i) the absorption spectra in the 1.2–1.6 μm interval; (ii) the emission spectra in the 1.5 μm spectral region; (iii) the absorption spectra in the pumping region around 1 μm; (iv) the fluorescence lifetime of the long lived $^4I_{13/2}$ level of the Er^{3+} ion (upper level for the 1.5 μm transition); (v) the ESA from the $^4I_{13/2}$ level. From these detailed investigations we derived interesting information on the shape of absorption and emission bands due to the local field felt by the Er^{3+} ions, line broadening mechanisms, efficiency of the pumping process at different wavelengths and we were able to calculate the absolute value of the spectral emission cross section at 1.5 μm.

2. Experiment

The experiments were performed using three samples with different dopant concentrations, supplied by Kigre. The glass base composition involves P_2O_5, ZnO, Al_2O_3, Er_2O_3 and, in codoped samples, Yb_2O_3. The first sample, hereafter denoted as sample A, is a commercial glass base named QE7, with nominal 1×10^{19} ions cm^{-3} Er^{3+} and 1×10^{21} ions cm^{-3} Yb^{3+}concentrations. Samples B and C are custom-made glass bases, designed with the aim of spectroscopic investigations, containing, respectively, Er and Yb ions with comparable concentrations (B) and only Er ions (C). The relative concentrations of the rare earths in these samples were derived from the absorption measurements, to be discussed in the following section, and are reported in Table 1.

For each sample, the absorption spectra were measured using a Perkin Elmer λ19 spectrophotometer. The emission spectra were measured at 90° with respect to the excitation beam through a Jobin Yvon H25 monochromator by an Hamamatsu cooled Ge detector. The excitation light was provided by a tungsten lamp filtered by a Jobin

Table 1
Rare earth-dopant concentrations in the three investigated samples

	Er^{3+}	Yb^{3+}
Sample A	10^{19} cm^{-3}	10^{21} cm^{-3}
Sample B	9×10^{19} cm^{-3}	5×10^{19} cm^{-3}
Sample C	1.5×10^{20} cm^{-3}	–

Yvon H10 monochromator or by an InGaAlAs laser diode (Opto Power, model OPC-A001-980-CT/100) tuned at 980 nm. The lifetime of the Er $^4I_{13/2}$ level (the upper laser level) was measured using a mechanically chopped laser-diode excitation and detecting the modulated fluorescence intensity as a function of the modulation frequency. All the above measurements were performed at different temperatures in the 10–300 K interval using a variable temperature, closed cycle, He cryostat.

3. Results and discussion

Fig. 1 shows a simplified energy level diagram of the Er–Yb system in phosphate glass and the processes of main interest for pumping in the 980 nm band in order to achieve optical amplification and laser action. In the following, we will present the results of our investigations for the processes of ground state absorption between the $^4I_{15/2}$ and $^4I_{13/2}$ manifolds, emission between $^4I_{13/2}$ and $^4I_{15/2}$ manifolds, ground state absorption between the $^4I_{15/2}$ and $^4I_{11/2}$ manifolds, and ESA from the $^4I_{13/2}$ manifold.

3.1. Absorption $^4I_{15/2} \rightarrow {}^4I_{13/2}$

The spectral region of the $^4I_{15/2} \rightarrow {}^4I_{13/2}$ transition is of particular interest because it lies at around the 1500 nm third optical telecommunication window. For a three-level gain system such as Er^{3+} at 1500 nm, in fact, not only the stimulated emission but also the absorption cross section play important roles in determining the performance of a device.

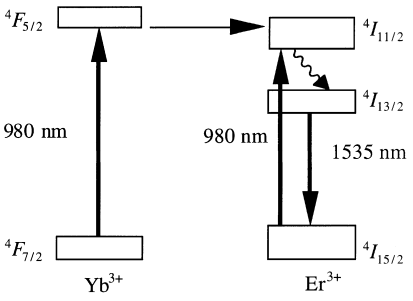

Fig. 1. Schematic representation of the levels involved in the optical processes. The solid line arrows indicate the absorption and emission transitions for the Er^{3+} and Yb^{3+} ions. The wavy lines represents the non-radiative decay $^4I_{11/2} \rightarrow {}^4I_{13/2}$ and the thin arrow stands for the energy transfer.

The absorption spectra of the three samples A, B, and C at $T = 10$ K are shown as solid lines in Fig. 2. The three spectra are fairly similar, the main difference arising from the sharper structures in sample C where the main peak shows a distinct splitting. From the intensity of the main absorption peaks the Er relative concentrations of the three samples is found to be proportional to 1:9:15. We assume that, at 10 K, only the lowest level of the $^4I_{15/2}$ manifold is populated, split by the local field of the ions surrounding the Er^{3+} dopant. Therefore the shape of the absorption curve should reflect the transition probabilities from the lowest ground state to the manifold of the $^4I_{13/2}$ excited state. The local Stark field splits

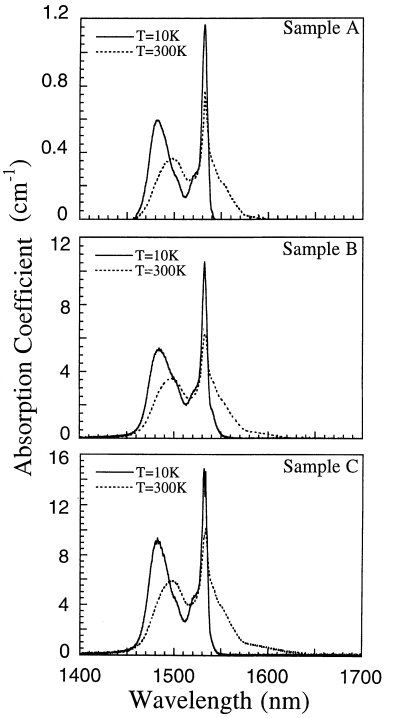

Fig. 2. Er^{3+} $^4I_{15/2} \rightarrow {}^4I_{13/2}$ absorption spectra, measured at 10 K (solid lines) and room temperature (dashed lines), of the three samples.

this manifold into seven states and thus we should observe an absorption line-shape consisting of a sum of seven Gaussian bands. Even if some structures are present in the line-shapes of Fig. 2 we cannot assign with certainty the observed peak positions to the seven Er^{3+} expected transitions. In fact, each transition is inhomogeneously broadened due to the presence of different local sites for the Er ions, each site absorbing at slightly different energy. Some general remarks can however be made based on the results of Fig. 2:

- the total splitting of the $^4I_{13/2}$ manifold is of the order of 250 cm^{-1}, very similar to the results obtained in several crystalline hosts (BaY_2F_8 [17], YSGG [18], $CaYAlO_4$ [19]),
- the transition at lower energy are in all three samples much narrower than those at higher energy. No explanation is at present available for the different behaviour of the lower and the higher energy transitions of the crystal field split $^4I_{13/2}$ manifold.

However, the marked difference in width of the lower energy bands with respect to the higher energy bands is also present in the case of BaY_2F_8 single crystal doped with Er [17]. In the crystalline host all the lines are perfectly resolved and therefore the different width of the bands may be related to an intrinsic property of the Er wave functions.

Upon increasing the temperature from 10 K to room temperature, one observes the rising of the absorption tail on the low energy side of the main peak, and a variation of the shape on the high energy side, together with a shift towards lower energies of the second peak at about 1490 nm (see Fig. 2). Both effects are clearly related to the thermal population of the higher levels of the ground state manifold, which brings to 56 the number of potentially observable transitions at high temperature. Apart from the change of the overall shape of the absorption band, at wavelengths shorter than 1530 nm we did not observe any sensible broadening of the absorption line-shape upon increasing the temperature. Inhomogeneous broadening, induced by the different local fields at the ion sites inside the glass matrix, appears thus to be the major contribution to the absorption line-shape. A temperature dependent homogeneous broadening, however, can be of some relevance in the case of the sharp peak at about 1530 nm and at longer wavelengths, although no quantitative estimates can be drawn, due to the overlap with transitions from and to different components of the two multiplets involved. A similar behaviour was found also for the $^4I_{13/2} \rightarrow {}^4I_{15/2}$ transitions, responsible for the emission spectra to be discussed in the next section. Upon a further increase in the temperature we therefore do not expect any sensible increase in the widths of both the absorption and emission bands, as compared with those observed at room temperature.

3.2. Emission $^4I_{13/2} \rightarrow {}^4I_{15/2}$

As already mentioned in the introduction, this transition is of the utmost importance as far as the Er-doped glass is used as active material to achieve optical amplification. The large bandwidth of this transition is in fact desirable for tuneable lasers to have a wide wavelength range over which they deliver relatively constant power. Similarly, optical amplifiers are more useful if they provide gain that is relatively independent of signal wavelength. This relaxes the wavelength tolerances on transmitters in a single-channel system, and increases the number of optical channels that can be multiplexed without gain compensation techniques in wavelength division multiplexed systems.

We analysed the temperature dependence of the emission line-shape for this transition upon excitation by an InGaAlAs laser diode tuned at 980 nm. At low temperature one can assume that only the lowest level of the $^4I_{13/2}$ manifold is populated, following the energy transfer from Yb to Er and the subsequent fast relaxation process ($\sim$1 μs) from the excited $^4I_{11/2}$ of Er^{3+} ions. The transitions from the lowest $^4I_{13/2}$ to the Stark split $^4I_{15/2}$ level should give rise to eight bands. Being at present impossible to perform in our laboratory Fluorescent Line Narrowing Experiments [20] in order to better resolve the emission line shape, we cannot accurately determine the position of the Stark sublevels and their dependence on the site selective excitation.

The results obtained in the three samples (Fig. 3) are fairly close to each other again showing a

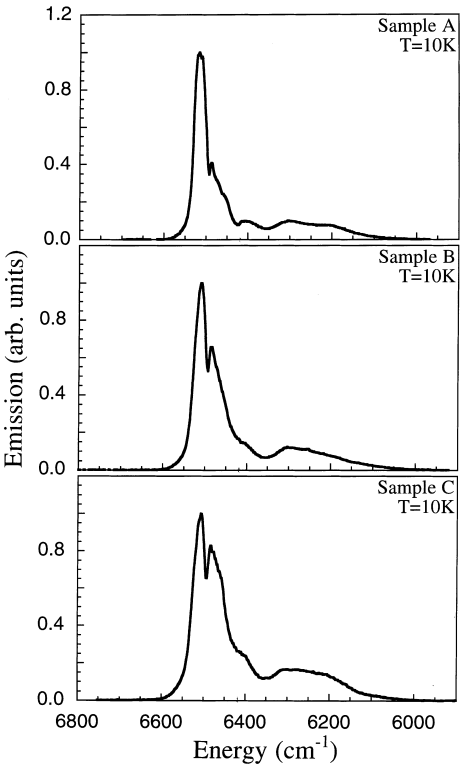

Fig. 3. Emission spectra measured at 10 K of the Er^{3+} $^4I_{13/2} \rightarrow {}^4I_{15/2}$ transition for the three samples.

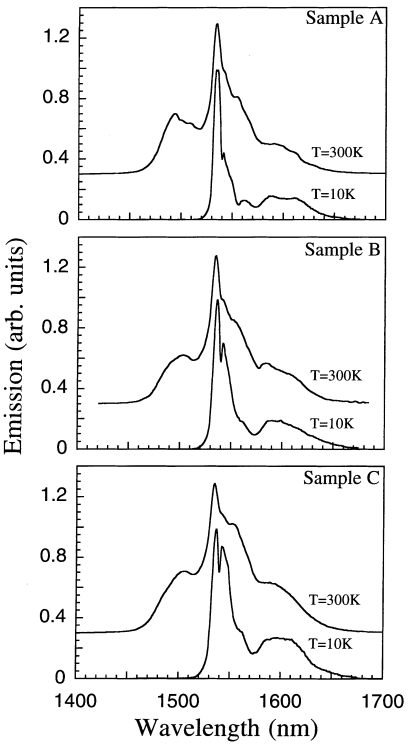

Fig. 4. Er^{3+} $^4I_{13/2} \rightarrow {}^4I_{15/2}$ emission spectra for the three samples at $T = 10$ K and at room temperature.

broader half-width of the transitions related to the higher levels of the $^4I_{15/2}$ manifold (i.e., those at lower energy) moreover a clear trend is evident showing a relative increase of the intensities of all the bands at lower energy with respect to band at 6520 cm^{-1} with increasing Er content in the glass base. Yb concentration does not seem to influence the emission spectra at low temperature, even if a greater number of samples with different Yb concentrations would be necessary to further clarify this point.

At higher temperatures the width of the emission band increases dramatically for the three samples, as well apparent from the spectra recorded at room temperature shown in Fig. 4. Because of the different weights of the emission sub-bands, the measurement of the overall spectral widths does not provide, however, relevant information: the huge variation of the shape of the emission spectra at high temperature is in fact mainly due to the onset of new transitions from several thermally populated excited states of the $^4I_{13/2}$ manifold. The spectra at room temperature in Fig. 4 show, indeed, also a relative intensity increase with temperature of the bands located at lower energies with respect to the emission peak. On the other hand, at energies higher than that of the peak, new emission sub-bands become increasingly populated with temperature. The overall emission bandwidth (full width at 1/e of the peak intensity) turns out to be about three times larger at room temperature than at 10 K. As a final note, from the spectra of Fig. 4 we observe that, also at room temperature, the intensity of the emission sub-bands at lower frequencies increases with Er concentration, while at higher frequencies the emission sub-bands appear more intense and structured in the glass with the highest Yb content (sample A). It can be inferred therefore that, at room temperature, the energy transfer process

from Yb to Er favours the population of the higher excited levels of the $^4I_{13/2}$ Er manifold.

To provide a comprehensive evaluation of the emission properties of the Er and Er–Yb-doped phosphate glasses, we also measured the fluorescence lifetime of the $^4I_{13/2}$ Er excited state and we calculated for the three samples the stimulated emission cross section with the method of $\beta-\tau$ integral [21], which relies only on the measurements of the spontaneous emission $I(\lambda)$ as a function of the wavelength and of the fluorescence lifetime τ_f. The fluorescence lifetime was measured at 10 K and at room temperature by measuring the fluorescence intensity as a function of the modulation frequency of the pump, and the results for the three samples are shown in Table 2.

The spectral emission cross section $\sigma(\lambda)$ can be determined using the following relationship [21]:

$$\sigma(\lambda) = \frac{\eta \lambda^5}{8\pi n^2 c \tau_f \int \lambda I(\lambda)\,d\lambda} I(\lambda), \quad (1)$$

where η is the branching ratio for the radiative decay, λ the emission wavelength, n the refractive index of the glass, and c the velocity of light in vacuum. In the above relation the ratio of the emission intensity $I(\lambda)$ to its integral value (as calculated in the denominator) makes the results for $\sigma(\lambda)$ independent of the geometry and of the absolute calibration of the detection system. By assuming in phosphate glass $\eta = 1$ and by using the measured lifetimes reported in Table 2, we were able to obtain a quantitative evaluation of $\sigma(\lambda)$ for the three samples at low (10 K) and room temperature. The results for the peak emission cross sections and the corresponding wavelengths at room temperature are reported in Table 3 and turn out to be in good agreement with those of other Er-doped phosphate glasses already quoted in the literature, shown for comparison in the same table.

Table 2
Lifetime τ_f of the Er^{3+} emission $^4I_{13/2} \rightarrow {}^4I_{15/2}$ for the three samples at 10 K and at room temperature. $\lambda_{exc} = 980$ nm

Temperature (K)	Sample A τ_f (ms)	Sample B τ_f (ms)	Sample C τ_f (ms)
10	9.8 ± 0.5	9.9 ± 0.5	7.0 ± 0.5
300	7.7 ± 0.5	7.5 ± 0.5	5.1 ± 0.5

Table 3
Stimulated emission cross section and peak wavelength of the investigated samples and of other phosphate glasses doped with Er and Yb

Sample	λ (nm)	σ_{max} (10^{-21} cm^2)	Ref.
Sample A-QE7	1535	7.7 ± 0.5	Present data
Sample B	1535	7.6 ± 0.5	Present data
Sample C	1535	8.9 ± 0.9	Present data
QE7	1535	8.0	[22]
Phosphate–Na–Mg	–	8.2	[10]
Phosphate LGS-E	–	7.7	[10]
Phosphate LGS-E7	–	7.9	[10]

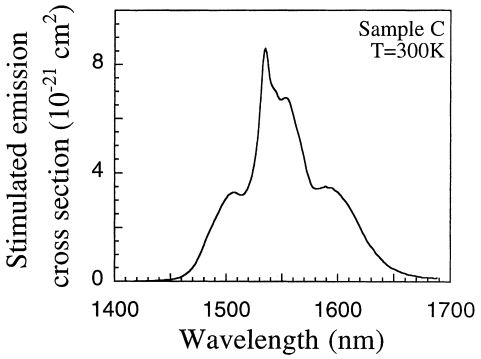

Fig. 5. Stimulated emission cross section of sample C at room temperature.

In Fig. 5 the whole spectral emission cross-section as a function of wavelength is shown for sample C at room temperature.

3.3. Er $^4I_{15/2} \rightarrow {}^4I_{11/2}$ and Yb $^2F_{7/2} \rightarrow {}^2F_{5/2}$ absorption transitions

These transitions and the dopants absorption in the spectral region between 0.9 and 1 μm, where high power InGaAs laser diodes are available, are extremely important both in the case of direct pumping of Er-doped glasses and for the optimisation of the pumping conditions and the Yb to Er energy transfer process in codoped glasses. Er-doped optical amplifiers pumped in this band have in fact not only shown the best performance with respect to gain and gain efficiency, but have also

achieved near quantum-limited noise figures of about 3 dB and signal output powers in excess of 30 dBm. Laser outputs of several hundreds milliwatt have been demonstrated, with optical to optical efficiency larger than 50%. This success is due to the large absorption cross sections of both Er and Yb for this band, coupled with the absence of excited state absorption (ESA) from the $^4I_{13/2}$ Er level in this wavelength interval, to be discussed in the following.

To investigate the main spectral features of both transitions, we measured the absorption spectra of the three samples at low temperature (10 K), which are shown in Fig. 6. The absorption spectrum of sample C, related only to the $^4I_{15/2} \rightarrow {}^4I_{11/2}$ Er transition, shows a split absorption band at 969 and 978 nm with a peak absorption coefficient of about 8 cm^{-1}. In samples A and B the two Er bands are superimposed to those of Yb. The main Yb band at 975 nm is accompanied with at least three higher-energy bands at 960, 935 and 916 nm. These latter bands do not overlap those of Er and, from their peak intensities, we deduced that the Yb content of sample A is about 20 times larger than that of sample B. Using the ions content of sample A as a reference, we calculated the concentration values reported in Table 1. From the intensities of the Er and Yb absorption bands in the 970–980 nm interval in sample B and the concentrations of both ions reported in Table 1, we could then estimate that the absorption cross sections of the two rare earth ions in these bands are of the same order of magnitude, at odd with the results quoted in Ref. [22].

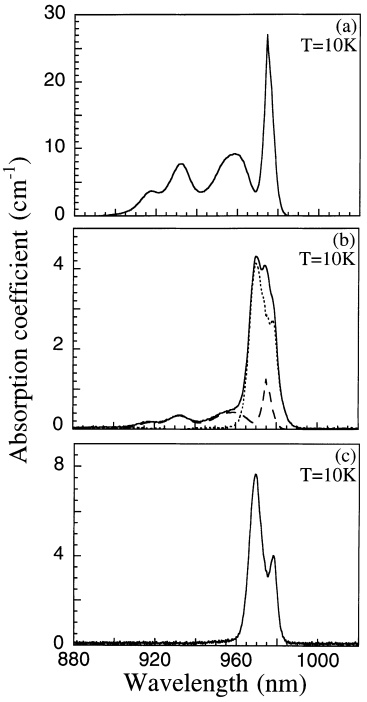

Fig. 6. Absorption spectra in the 980 nm band of sample A (a), sample B (b, solid line) and sample C (c). In (b) it is also shown the contribution of Er^{3+} to the absorption spectrum (dots), obtained by subtracting the Yb^{3+} absorption spectrum (dashed line).

3.4. Excited state absorption from $^4I_{13/2}$

A main dissipative process in Er-doped glasses used as active materials at 1.5 μm is the excited-state absorption (ESA) from the metastable $^4I_{13/2}$ level. In fact photons absorbed in transitions originating from the $^4I_{13/2}$ level result are lost, being the excitation energy released through fast non-radiative processes. A detailed investigation of ESA is of great important for a proper choice of the pump wavelength. Indeed, ESA of pump photons strongly affect the pumping efficiency [23,24]. We performed accurate ESA measurements by pumping the sample with 980 nm radiation and testing the pump-induced absorption in the 450–1200 nm wavelength interval to cover all pump wavelengths of interest. In Fig. 7 we show the comparison between the ground-state absorption (GSA, dashed line) and the pump induced change in the absorption coefficient (ESA, solid line). A positive change means that absorption cross section of the $^4I_{13/2}$ is greater than the absorption cross-section of $^4I_{15/2}$. The negative signal reflects the decrease of the absorption due to the depleted population of the ground state $^4I_{15/2}$. From Fig. 7 we can conclude that 980 nm radiation does not suffer from ESA and it is suitable as an effective pump wavelength. The other promising candidate, the 800 nm pump band, is affected at its blue edge by ESA, which decreases the pumping efficiency especially when the $^4I_{13/2}$ level is strongly populated as in high-loss cavity lasers.

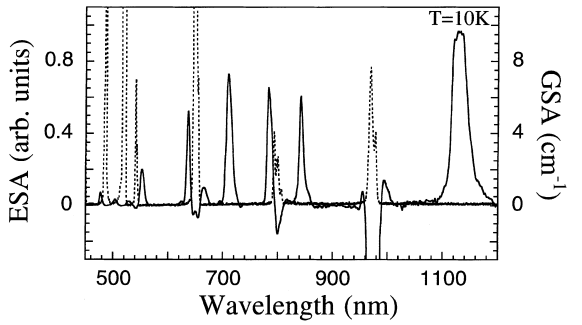

Fig. 7. Excited State Absorption (ESA, solid line) and Ground State Absorption (GSA, dashed line) spectra of sample C at 10 K.

Table 4
Final level and wavelength corresponding to the measured ESA transitions from the $^4I_{13/2}$ level

Final level	Wavelength (nm)		
	Sample A	Sample B	Sample C
$^2G_{9/2}$	477	478	478
$^4G_{11/2}$	503	504	504
$^2H_{9/2}$	553	552	552
$^4F_{5/2}$–$^4F_{3/2}$	635	637	637
$^4F_{7/2}$	708	708	710
$^2H_{11/2}$	782	783	782
$^4S_{3/2}$	841	842	841
$^4F_{9/2}$	1136	1127	1126

Table 4 summarises the ESA transitions for the three samples. It may be noted that samples A and B do not show any special feature due to Yb co-doping. Nearly all observed ESA bands coincide with those reported in the literature [1]. In addition we observed few extra bands in the region of high energies. As compared with [1] we note a slightly down shifting of 5–10 nm of our band peaks till the 708 nm transition and a 5 nm red shift for the $^2H_{9/2}$ ESA transition peak wavelength. We attribute the slightly reported differences to the somewhat arbitrary deconvolution of the contributions of ESA and GSA absorption spectra.

4. Conclusions

The spectroscopic properties of Er and Er–Yb-doped glasses in three samples with different ions concentrations were thoroughly investigated at low and room temperature with the aim of getting further insights on the energy levels, crystal field interactions and line broadening mechanisms in phosphate glasses. In addition, the $^4I_{13/2}$-fluorescence lifetime was carefully measured and the stimulated emission cross sections were determined. Ground state absorption (GSA) spectra in the 980 nm pump band at low temperature were recorded and accurate ESA measurements after excitation at 980 nm were also performed. The results obtained provide useful guidelines for the choice of Er and Yb concentrations as well as for modelling and optimising the performance of lasers and optical amplifiers based on Er-and Er–Yb-doped phosphate glasses.

References

[1] W.J. Miniscalco, Optical and electronic properties of rare earth ions in glasses, in: M.J.F. Digonnet (Ed.), Rare Earth Doped Fiber Lasers and Amplifiers, Marcel Dekker, New York (Basal), 1993.
[2] E. Desurvire, Erbium Doped Fiber Amplifiers, Wiley, 1994.
[3] S. Najafi, Overview of Nd-and Er-doped glass integrated optics amplifiers and lasers, in: S. Hankanen (Ed.), Rare-Earth-Doped Devices, Proceedings of SPIE, 2296, 1997.
[4] D.C. Hanna, A. Kazer, D.P. Shepherd, OPt. Commun. 63 (1987) 417.
[5] J.E. Towsend, W.L. Barnes, K.P. Jedryejewski, S.G. Grubb, Electronic Lett. 27 (1991) 1958.
[6] X. Zoin, T. Izumitani, J. Non-Cryst. Solids 162 (1993) 68.
[7] Y.-L. Lu, Y.-Q. Lu, N.-B. Ming, Appl. Phys. B 62 (1996) 287.
[8] T. Catunda, L.A.O. Nunes, A. Flores, Y. Messaddeq, M.A. Aegerter, Phys. Rev. B 53 (1996) 6065.
[9] E. Snitzer, R. Woodcock, Appl. Phys. Lett. 6 (1965) 45.
[10] R.J. Mears, L. Reekie, I.M. Jauncey, D.N. Payne, Electron. Lett. 23 (1987) 1026.
[11] V.P. Gapontsev, S.M. Matisin, A.A. Iseneev, V.B. Kravchenko, Opt. Laser Technol. 14 (1982) 189.
[12] J.C. Wright, Topics in Applied Physics, in: F.K. Fong (Ed.), Radiationless Processes in Molecules and Condensed Phases, Springer, Berlin, 1976.
[13] P. Laporta, S. De Silvestri, V. Magni, O. Svelto, Opt. Lett. 16 (1991) 1952.
[14] J.A. Huttchinson, T.H. Allik, Appl. Phys. Lett. 60 (1992) 1424.
[15] J.T. Kringlebotn, P.R. Morkel, L. Rekiee, J.L. Archambault, D.N. Payne, IEEE Photon. Technol. Lett. 5 (1993) 1162.

[16] K. Hsu, C.H. Miller, J.T. Kringlebotn, D.N. Payne, Opt. Lett. 20 (1995) 337.
[17] R. Capelletti, private communication.
[18] P.F. Multon, J.G. Manni, G.A. Rines, IEEE J. Quantum Electron. 24 (1988) 960.
[19] J.C. Souriau, C. Borel, C. Wyon, C. Li, R. Moncorgé, J. Lumin. 59 (1994) 349.
[20] S. Zemon, G. Lambert, L.J. Andrews, W.J. Miniscalco, B.T. Hall, T. Wei, R.C. Folweiler, J. Appl. Phys. 69 (1991) 6799.
[21] B.F. Aull, H.P. Jenssen, IEEE J. Quantum Electron QE-18 (1982) 925.
[22] M.P. Helen, N.J. Cockroft, T.R. Gosnell, A.J. Bruce, Phys. Rev. B 56 (1997) 9302.
[23] W.J. Miniscalco, J. Lightwave. Technol. 9 (1991) 234.
[24] S. Jiang, J. Myers, D. Rhonehouse, M. Myers, R. Belford, S. Hamlin, SPIE, 2138, 1994.